Journal of Non-Crystalline Solids 378 (2013) 196–200

Contents lists available at SciVerse ScienceDirect

Journal of Non-Crystalline Solids

journal homepage: www.elsevier.com/ locate/ jnoncrysol

Electronic conductivity of vanadium-tellurite glass-ceramics

Jonas Kjeldsen [a], Yuanzheng Yue [a,*], Caio B. Bragatto [b], Ana C.M. Rodrigues [b,**]

[a] Section of Chemistry, Aalborg University, DK-9000 Aalborg, Denmark
[b] Department of Materials Engineering, Federal University of São Carlos, C.P. 676, 13565-905 São Carlos, SP, Brazil

ARTICLE INFO

Article history:
Received 27 February 2013
Received in revised form 25 June 2013
Available online xxxx

Keywords:
Glass-ceramics;
Vanadium tellurite;
Electronic conductivity;
Cathode materials;
Glass transition temperature;
Percolation

ABSTRACT

In this paper, we investigate the electronic conductivity of $2TeO_2$–V_2O_5 glass-ceramics with crystallinity ranging from 0 to 100 wt.%, i.e., from entirely amorphous to completely crystalline. The glass is prepared by the melt quenching technique, and the crystal is prepared by subsequent heat treatment thereof. Glass-ceramics are prepared by mixing glass and crystal powder, followed by a sintering procedure. Activation energies for electronic conduction in the glass and in the crystal are determined by fitting the Mott–Austin equation to the electronic conductivity data obtained by impedance spectroscopy. We find similar activation energies for both glass and crystal, implying that they have similar conduction mechanisms, i.e., thermally activated hopping. The electronic conductivity of $2TeO_2$–V_2O_5 glass is about one order of magnitude higher than that of the corresponding crystal, and a percolation phenomenon occurs at a glass fraction of 61 wt.%, increasing from a lower conductivity in the crystal to a higher conductivity in the glass. We explain the behavior of electronic conduction in the $2TeO_2$–V_2O_5 glass-ceramics by considering constriction effects between particles as well as percolation theory. This work implies that, based on its electronic conductivity, vitreous $2TeO_2$–V_2O_5 is more suitable as a cathode material in secondary batteries compared to a $2TeO_2$–V_2O_5 glass-ceramic.

1. Introduction

Batteries are essential in modern society to sustain our high-tech lifestyles. Since a large segment of the world's population utilizes electronics powered by batteries every day, both available technologies for batteries and prospects for future technology are objects of extensive research. As an excellent source of mobile energy, batteries are receiving a large amount of attention compared to other available technologies.

Lithium is both the most electro-positive (−3.04 V vs. a standard hydrogen electrode) as well as the lightest metal and therefore has the strongest potential for designing batteries with a high energy density [1]. For high power electrochemical cells, it is important that the electronic conductivity in the electrodes is high and that there is a rapid change in charge carriers at the electrolyte/electrode interface (transfer from lithium ions in the electrolyte to electrons in the electrodes) [2]. Considering these requirements, the use of an amorphous mixed conductive electrode material has been proposed [2], i.e., an amorphous material that is able to conduct a current by both electrons and ions. Since V_2O_5–TeO_2 glass may intercalate lithium ions [3], the use of lithium-intercalated V_2O_5–TeO_2 may present several advantages: First, the change in charge carriers is not confined to the surface of the electrode but can extend through the material, which increases the number of sites available for transfer. Second, in an amorphous electrode, the electro-active species is separated from the electron and occupies well-defined cationic sites. When dissolved in this manner, the electro-active species is considered to be intercalated, and its chemical potential is far less than that of the pure species [2]. This difference in chemical potential is the driving force for current flow in a battery and is therefore highly important for the design of highly energy dense electrochemical cells. Third, when comparing amorphous and crystalline structures, degradation during consecutive lithiation cycles (repetitions of charging and discharging) is lowest in an amorphous material [2]. Compared to a crystalline material, the structural units in a glass are easier to rearrange, and thus, the glass is more resistant to the degradation caused by expansion during lithiation cycles.

The most common cathode material in secondary lithium batteries is $LiCoO_2$. However, $LiCoO_2$ only has a moderate energy density (measured in kWh/kg), and the CoO_2 layers created during delithiation (charging) are sheared from the electrode surface, which reduces the energy density because fewer lithium sites are available for lithiation [4]. Cobalt, which is both expensive and toxic, is also dissolved in the electrolyte during delithiation [5]. Due to the listed limitations of the current cathode material, it is of interest to find another material with superior properties. Lithium vanadiotellurite is a mixed conductor that previously has been suggested for use as a cathode material [2,3,6,7]. Vanadium tellurite is able to intercalate lithium ions and experiences high electronic conductivity compared to other binary or ternary vanadium compounds [2,8–21]. Because electronic conduction

* Corresponding author. Tel.: +45 9940 8522.
** Corresponding author. Tel.: +55 16 3351 8556.
E-mail addresses: yy@bio.aau.dk (Y.Z. Yue), acmr@ufscar.br (A.C.M. Rodrigues).

0022-3093/$ – see front matter © 2013 Elsevier B.V. All rights reserved.
http://dx.doi.org/10.1016/j.jnoncrysol.2013.07.011

occurs by electron hopping from one vanadium ion to another, theoretically, the highest electronic conductivity is achieved in pure vanadium oxide, simply because the distance between adjacent vanadium ions is minimized. Hirashima et al. [22] postulate that the conductivity of a vanadium tellurite crystal might be as high as that of a divanadium pentoxide crystal and that both are 2 orders of magnitude larger than that of the corresponding glass. The synthesis of congruent $2TeO_2$–V_2O_5 crystals has been reported [6,23–31], but to the best of our knowledge, the electronic conductivity of either the crystal or the mixtures between glassy and crystalline $2TeO_2$–V_2O_5 has not been measured. Therefore, in this paper, we investigate the dependence of the electronic conductivity on the weight % of glass in different mixtures of congruent $2TeO_2$–V_2O_5 crystal and glass.

2. Experimental

Glass samples were prepared via the normal melt quenching technique using reagent grade ≥99.6% V_2O_5 and ≥99.5% TeO_2. Appropriate amounts for obtaining $2TeO_2$–V_2O_5 were mortared, and 12 g was melted in a gold crucible at 700 °C for 1 h. The melt was quenched on a brass block and annealed for 2 h at 250 °C. Differential scanning calorimetry (DSC) (Netsch, DSC404) at 1 K/min was performed up to 400 °C on a solid sample using gold crucibles. Heat treatment was conducted at 400 °C for 2 h in order to crystallize the glass, and both crystalline and glassy samples were examined with a scanning electron microscope (SEM) (Phenom). Images were taken on the surface of the samples and in fractures (the interior of the samples). Different ratios of glass and crystal were mixed to obtain nine samples with a glass fraction ranging from 0 to 100 wt.%. Each sample was pressed under 20.6 MPa and sintered for 2 h at 270 °C. All samples were disc shaped with a diameter of 1.8 mm and a height of 1 mm. The temperature of sintering (T_s) was obtained with an optical dilatometer (Misura, HSM-ODHT) measuring 2-dimensional shrinkage during scans from 298 to 673 K with scanning rates of 2, 5 and 10 K/min. T_s is then defined as the temperature where the largest volume shrinkage occurs. SEM images were taken of these glass-ceramic samples. The samples were polished, and gold was sputtered on the parallel surfaces before the electronic conductivity was measured by impedance spectroscopy (IS) (Solartron, SI1260). The electrical measurements were performed in air with a two-point sample holder from 303 to 523 K and with an applied voltage of 100 mV in the frequency range from 10^6 to 1 Hz. X-ray diffraction (XRD) (Rigaku, Ultima IV) using Cu K_α-radiation was applied at room temperature on all samples in order to confirm their amorphous or crystalline states. Scans were conducted at 0.02°/s from 10 to 90°.

3. Results & discussion

Fig. 1 shows the DSC curve of the $2TeO_2$–V_2O_5 glass, from which the glass transition temperature (T_g) and the crystallization temperature (T_c) are determined to be 251 and 400 °C, respectively. T_c is determined from the crystallization peak position, whereas T_g is determined from the onset temperature of the glass transition [32,33]. The $2TeO_2$–V_2O_5 glass crystallizes around a single distinctive temperature, indicating the formation of one single crystalline phase. The T_g and T_c values agree well with those reported in the literature [13,25,30]. Figs. 2 and 3 show the XRD patterns and scanning electron microscopy images of both glassy and crystalline $2TeO_2$–V_2O_5 (the crystalline phase was obtained by heat treatment at 400 °C for 2 h). The XRD pattern confirms the amorphous nature of the sample before heat treatment due to the lack of Bragg peaks [34]. Fig. 2(b) and (c) shows that the XRD pattern of the analyzed sample coincides with the pattern of $2TeO_2$–V_2O_5 from the Joint Committee on Powder Diffraction Standards (card no. 71-0719) [25,29], indicating that the crystal obtained in this work is $2TeO_2$–V_2O_5. SEM images were taken of both glass and crystal (Fig. 3). As shown in Fig. 3, the glassy sample contains no

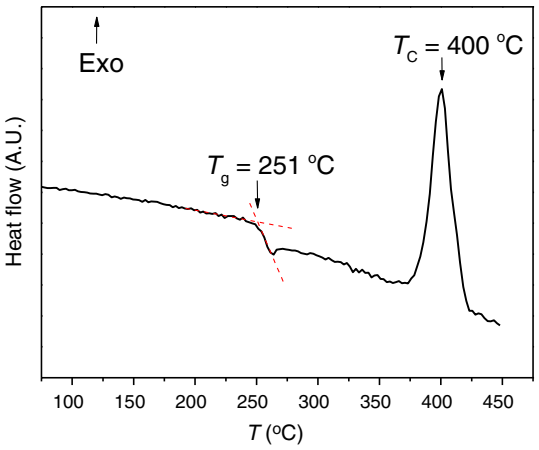

Fig. 1. A DSC scan of $2TeO_2$–V_2O_5 glass at a scanning rate of 1 K/min. Glass transition temperature (T_g) and crystallization temperature (T_c) are marked on the figure.

detectable crystals (Fig. 3(a)), and the crystalline sample contains no detectable vitreous phase either on the surface (Fig. 3(b)) or in the bulk (Fig. 3(c)); thus, the vitreous sample is fully amorphous, and the crystalline sample is completely crystallized.

The mixed glassy and crystalline samples are sintered at T_s = 543 K. As shown in Fig. 4, this temperature corresponds to that of the largest volume shrinkage and, hence, the highest sintering rate. Moreover, T_s is independent of the heating rate, and sintering starts almost immediately after the temperature is raised above T_g. Sintering, which is driven by a diffusion of atoms, occurs immediately after the temperature exceeds T_g due to a fast drop in viscosity upon heating, which indicates a fragile liquid. Fig. 4 shows that an expansion occurs at temperatures higher than T_s, which is attributed to the release of trapped air. At high heating rates, the time for the trapped air to be released is so short that the expansion becomes more pronounced (Fig. 4).

We analyzed a vitreous bulk sample and a vitreous sintered sample, i.e., a sample made by sintering glass powder following the sintering conditions described above, and found identical electronic conductivity for the two samples. XRD data confirm that both the bulk and the sintered powder samples are amorphous. Both samples present the same electrical conductivity, so the applied sintering process does not induce crystallization (which was expected based on Fig. 1.) and does not change the electronic conductivity. In Fig. 5, the electronic conductivity of a vitreous and a crystalline bulk sample is plotted against the inverse temperature. Earlier measurements combined with those presented in this paper show that by increasing the melting temperature, the electronic conductivity can be increased by 2 orders of magnitude [13–15]. Since an increase in melting temperature reduces the valence state of the vanadium in the melt, the

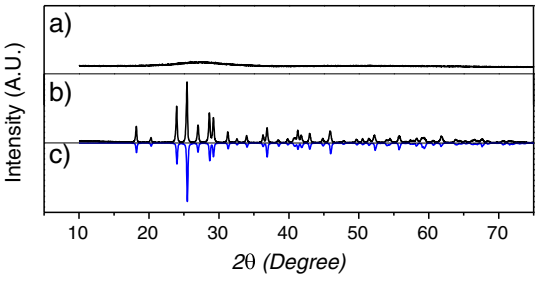

Fig. 2. X-ray diffraction patterns of (a) $2TeO_2$–V_2O_5 glass produced in this work, (b) $2TeO_2$–V_2O_5 crystal produced in this work, and (c) $2TeO_2$–V_2O_5 crystal from [29]. For better comparison between the crystal produced in this work and the crystal presented in [29], their pattern has been inversed (Fig. 2(c)).

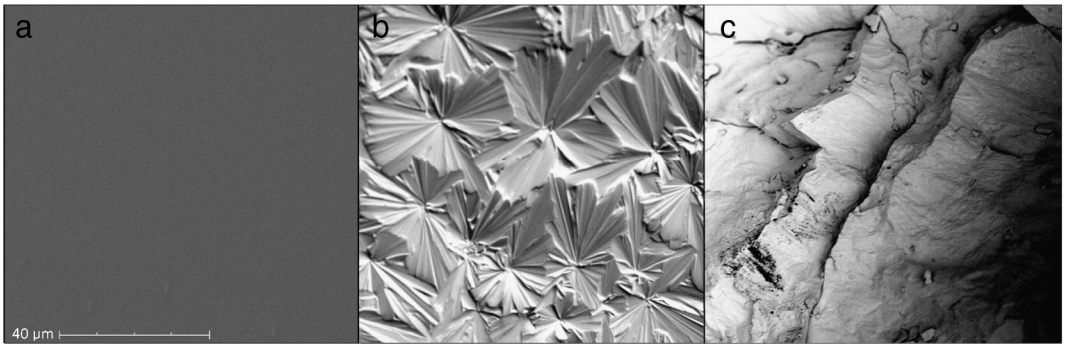

Fig. 3. Scanning electron microscopy images of (a) the surface of $2TeO_2$–V_2O_5 glass, (b) the surface of $2TeO_2$–V_2O_5 crystal, and (c) the fracture of $2TeO_2$–V_2O_5 crystal. The three images are taken with similar settings but (c) is taken at a lower magnitude compared to (a) and (b).

melting and annealing conditions are crucial parameters for varying the electronic conductivity. Therefore, a comparison of the electronic conductivity between two samples is only meaningful when they have identical thermal histories, as is the case for the samples presented in Fig. 5.

Electronic conductivity data were fitted using an equivalent circuit consisting of one resistor in parallel with one capacitor. By using a Levenberg–Marquardt algorithm, the variables from the equivalent circuit are fitted to the impedance data presented in a Nyquist plot, and the resistance of the sample is determined [35,36]. An example of the obtained IS data is shown in the inset of Fig. 5. The electronic conductivity (σ) is calculated using Eq. (1).

$$\sigma = \frac{1}{R_s}\cdot\frac{l}{A} \tag{1}$$

where l is the thickness of the sample, A is the area of the electrode in contact with the sample, and R_s is the resistance of the sample [13,37]. As shown in Fig. 5, the temperature dependence of $\log(\sigma T)$ follows a linear tendency and can therefore be approximated by the Mott–Austin equation [38,39].

$$\sigma = \left(\frac{\nu e^2}{Rk_bT}\right)c(1-c)e^{-2\alpha R}e^{-\frac{W}{k_bT}} \tag{2}$$

where ν is the optical phonon frequency, R is the mean distance between the ions where the electron transfer occurs (vanadium ions in this case), c is the concentration of these ions, α is the tunneling factor and W is the activation energy, which is split into two terms depending on temperature.

$$W = \begin{cases} W = W_H + \frac{1}{2}W_D & \text{for } T \geq \frac{1}{2}\Theta_D \\ W = W_D & \text{for } T \leq \frac{1}{4}\Theta_D \end{cases} \tag{3}$$

where W_H is the polaron hopping energy, W_D is the energy of disorder and Θ_D is the Debye temperature. The solid lines in Fig. 5 are Mott–Austin fits (Eq. (2)), from which the activation energies can be determined. The slopes of the straight lines are similar, which indicates that the activation energies are similar. The activation energies of the glass and the crystal are $W_{glass} = 0.39 \pm 0.03$ eV and $W_{crystal} = 0.42 \pm 0.03$ eV, respectively. The activation energies are determined using electronic conductivities in a temperature range from 303 to 523 K, which is much higher than $1/2\Theta_D$ [40], so the electronic conduction occurs by thermally activated hopping (Eq. (3)) [38]. Since the difference in activation energy between the two samples is within the error range, the mechanisms of electron transfer for the two samples are likely similar. The activation energy calculated for conduction in the glass is in good agreement with what have been reported in the literature, $W_{glass} = 0.42 \pm 0.08$ eV [13–15].

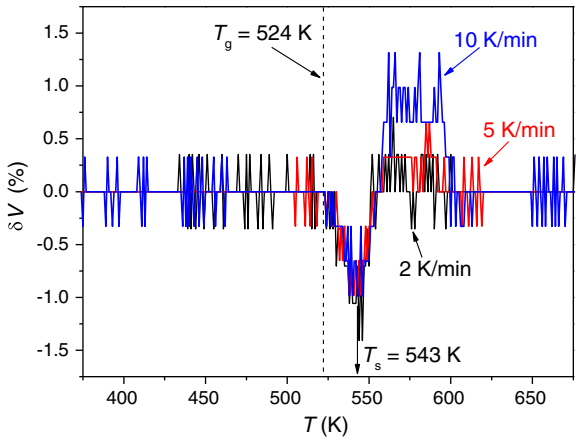

Fig. 4. Volume changes (δV) as a function of temperature measured with a heating microscope. The samples are vitreous $2TeO_2$–V_2O_5 with a starting volume of 2.5 mm^3. Isotropic shrinkage is assumed, and the heating rates are marked on the figure along with the sintering temperature (T_s) and the glass transition temperature (T_g).

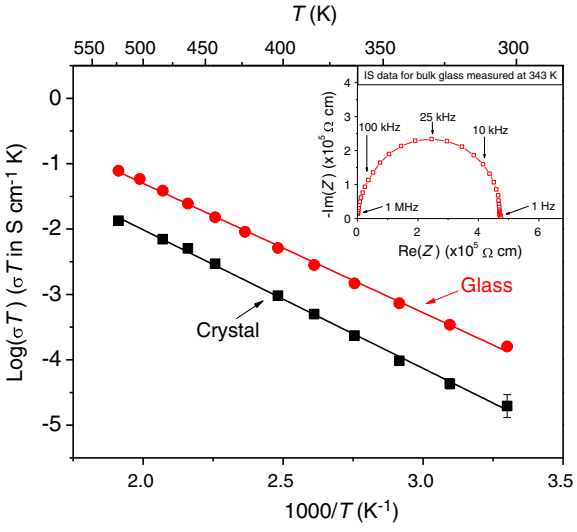

Fig. 5. $\log(\sigma T)$ as a function of the inverse temperature for both bulk $2TeO_2$–V_2O_5 crystal and glass. Solid lines: Mott–Austin fits (Eq. (2)) [38,39] with a correlation factor of $r^2 = 0.998$ for both lines. Both samples were melted at 973 K for 1 h and annealed at T_g for 2 h. Inset: Example of a semicircle obtained for glassy $2TeO_2$–V_2O_5 by impedance spectroscopy at 343 K. Note the absence of any low frequency spike attributable to the polarization of the electrode–electrolyte interface. Its absence is characteristic of pure electronic conductivity (no ionic transport) [49].

The electronic conductivity of samples with crystallinity ranging from 0 to 1 is plotted against the inverse temperature in Fig. 6. The base glass of these samples experienced different annealing conditions from those whose electronic conductivity is presented in Fig. 5. Therefore, the electronic conductivities presented in Figs. 5 and 6 are not comparable. Fig. 6 shows that the electronic conductivity of the glass-ceramic samples increases with increasing temperature in a non-Arrhenian way. It should be mentioned that the Mott–Austin equation is applicable only for monophase structures and not for multi-phase systems, such as glass-ceramics [39]. This limitation is due to possible differences in the temperature dependence of activation energies for different phases.

Fig. 6 shows that the electronic conductivity increases with an increasing fraction of glass in the sample. This trend is better revealed in Fig. 7, where the electronic conductivity measured at different temperatures is plotted against the glass fraction in the samples. All four curves show the same overall trend of two plateaus separated by a transition zone. The crossover from low to high conductivity occurs at a glass fraction of about 61 wt.%. Another trend is that the enhancement of the electronic conductivity by increasing the glass fraction is more pronounced at low temperatures than at high temperatures (inset of Fig. 6). As the activation energy of the glassy phase is slightly higher than that of the crystal, a more pronounced difference in electrical conductivity at low temperatures is expected.

According to [38], the Mott–Austin equation (Eq. (2)) is only applicable for monophase systems. However, here, we show that the activation energies for the two different phases are constant in the entire temperature range of measurement, implying that the Mott–Austin equation could be applicable. All samples have comparable α and ν values (Eq. (1)) because they have identical chemical compositions. This leaves us with only two parameters, namely, c and R, which can be related to the dependence of the glass fraction on the electronic conductivity. This dependence results from either: changes in the redox state of vanadium in crystallized samples (reflected by changes in c) or limitation of the electronic conduction in the grain boundaries. A reduced conduction in grain boundaries has been shown for ionic conductors [41,42] and is attributed to a constriction effect caused by a small contact area between grains [43]. This may also be applied in the present case of electronic conduction in mixed crystalline and vitreous grains. The sigmoid shape of the curves (Fig. 7) indicates a percolation threshold, which could be caused by the lower intrinsic electronic conductivity in the crystal grains

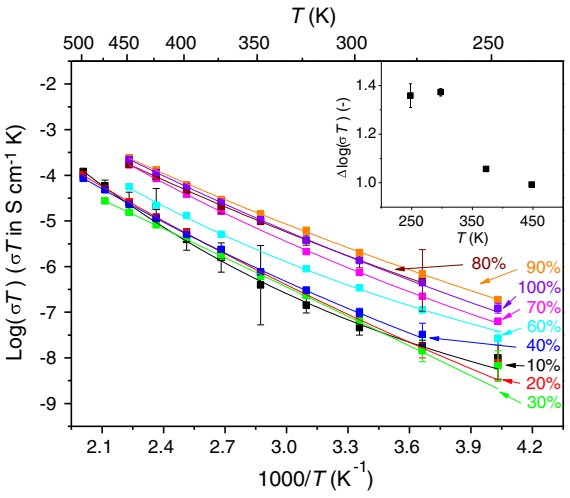

Fig. 6. Log(σT) as a function of the inverse temperature for different wt.% of glass in the glass-ceramic samples (marked on the curves), where σ is the electronic conductivity. The solid lines are guides for the eyes. Inset: $\Delta\log(\sigma T)$ as a function of temperature, where $\Delta\log(\sigma T)$ is the difference in $\log(\sigma T)$ between the sample containing 90 wt.% glass and that containing 10 wt.% glass.

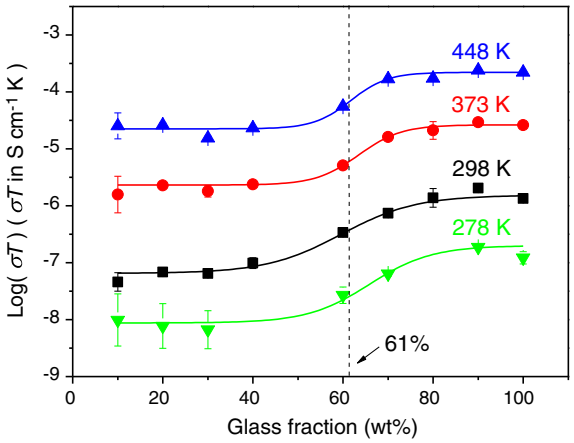

Fig. 7. Electronic conductivities measured at different temperatures (marked on the curves) as a function of the glass fraction in the $2TeO_2$–V_2O_5 glass-ceramic samples. Solid lines: sigmoid fits; Vertical dashed line: crossover point of the sigmoid curves.

compared to that in the glassy grains. Since the electronic conductivity is higher in the glassy grains than in the crystal grains, the glassy phase facilitates the electrons' preferred pathway. Fig. 7 suggests that an interconnected pathway of glass grains does not occur until the glass fraction reaches 61 wt.%, which agrees with the critical site percolation concentration (p_c) of 0.59 in a 2-dimensional square lattice [44–46]. However, a 3-dimensional network of randomly packed spheres has a p_c of 0.27 (16 vol.%) [45], whereas a 3-dimensional cubic lattice has a p_c of 0.31 [46]. These p_c values are inconsistent with the findings depicted in Fig. 7. If the conductivity jump illustrated in Fig. 7 originates from a percolation threshold, the system studied in this work would considerably differ from the ideal systems described by the models proposed in [45–47]. The cause of the measured p_c being relatively high could lie in either a small packing fraction of the glass-ceramic or a low average coordination number of the grains. Either cases alone or a combination hereof leads to an increase of apparent p_c [45,47,48]. From the SEM image in Fig. 8, it is difficult to determine the apparent particle size distribution or particle morphology and to make a link between the experimental system and the models described elsewhere [44–46]. In Fig. 8, it is not possible to distinguish between the glassy and crystalline grains, as the difference in electronic density between the two phases is too small. If possible, this would have provided important information about the percolation threshold. Using the critical glass fraction of 61 wt.%, we can infer that below this value, the electrons must travel through

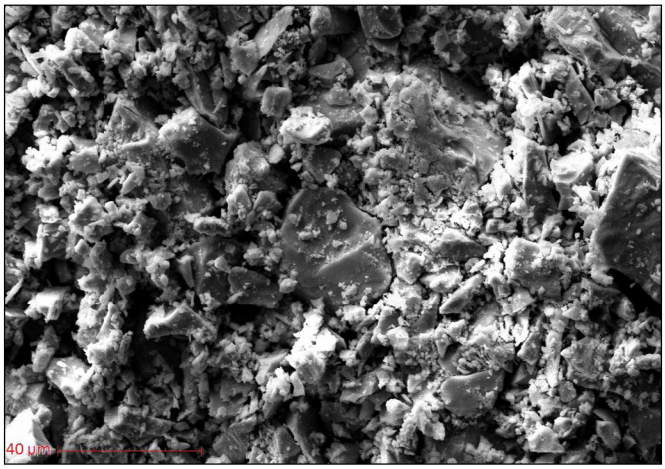

Fig. 8. SEM image of a glass-ceramic sample with a glass fraction of 30 wt.%. The image was taken in a fracture.

crystal regions of lower conductivity, thus reducing the overall electronic conductivity, whereas above this value an interconnected glass phase exists, and the electrons may therefore travel only in the glassy grains, increasing the electronic conductivity. Fig. 6 shows that the electronic conductivity of vitreous $2TeO_2$–V_2O_5 is up to 1.5 orders of magnitude higher than that of the crystal. This result is in contrast to results reported in [22], where the electronic conductivity of a $2TeO_2$–V_2O_5 crystal was 2 orders of magnitude higher than that of the corresponding glass. This discrepancy could be related to differences in the redox state of the vanadium ions in the samples in this work and in the samples investigated in [22]. It is also worth noting that the crystallized $2TeO_2$–V_2O_5 samples studied in [22] contained V_2O_5-crystals that may have contributed to the increased electronic conductivity of the $2TeO_2$–V_2O_5 glass-ceramic.

4. Conclusions

Activation energies for electronic conduction determined in the temperature range from 303 to 523 K in both vitreous and crystallized $2TeO_2$–V_2O_5 are found to be similar within experimental error, where $W_{glass} = 0.39 \pm 0.03$ eV and $W_{crystal} = 0.42 \pm 0.03$ eV. These results indicate that the mechanisms of electronic conduction are similar, i.e., thermally activated hopping. The electronic conductivity of vitreous $2TeO_2$–V_2O_5 is up to 1.5 orders of magnitude higher than that of the crystal, suggesting that $2TeO_2$–V_2O_5 glass is more suitable for use as a cathode material in secondary batteries than a $2TeO_2$–V_2O_5 glass-ceramic. The lower electronic conductivity of the glass-ceramic samples, compared to that of the amorphous one, is explained by constriction effects in the grain boundaries. A jump in electronic conductivity is observed at a glass fraction of 61 wt.%, and is attributed to a critical percolation concentration, which is higher than the theoretical value due to heterogeneities and flaws in the investigated system.

Acknowledgments

We thank the collaboration partners of the Department of Materials Engineering at Federal University of São Carlos for their help with sample preparation and characterization. Ana C. M. Rodrigues and Caio B. Bragatto acknowledge support from Fapesp, the São Paulo state funding agency. Ana C. M. Rodrigues acknowledges support from grant # 2007/08179-9, São Paulo State Research Foundation (Fapesp)-Brazil.

References

[1] A. Patil, V. Patil, D.W. Shin, J.-W. Choi, D.-S. Paik, S.-J. Yoon, Mater. Res. Bull. 43 (2008) 1913.
[2] M. Levy, J.L. Souquet, Mater. Chem. Phys. 23 (1989) 171.
[3] M. Levy, M.J. Duclot, F. Rousseau, J. Power Sources 26 (1989) 381.
[4] J.W. Fergus, J. Power Sources 195 (2010) 939.
[5] A.G. Ritchie, J. Power Sources 96 (2001) 1.
[6] P. Rozier, T. Dubois, P. Sallas, J. Non-Cryst. Solids 311 (2002) 241.
[7] M.A. Frechero, O.V. Quinzani, R.S. Pettigrosso, M. Villar, R.A. Montani, J. Non-Cryst. Solids 353 (2007) 2919.
[8] L. Murawski, R.J. Barczynski, Solid State Ionics 176 (2005) 2145.
[9] R.A. Montani, A. Robledo, J.C. Bazán, Mater. Chem. Phys. 53 (1998) 80.
[10] N. Lebrun, M. Levy, J.L. Souquet, Solid State Ionics 40/41 (1990) 718.
[11] M. Levy, F. Rousseau, M.J. Duclot, Solid State Ionics 28–30 (1988) 736.
[12] C.H. Chung, J.D. Mackenzie, J. Non-Cryst. Solids 42 (1980) 357.
[13] M.M. El-Desoky, Mater. Chem. Phys. 73 (2002) 259.
[14] G.D.L.K. Jayasinghe, M.A.K.L. Dissanayake, M.A. Careem, J.L. Souquet, Solid State Ionics 93 (1997) 291.
[15] R.A. Montani, A. Lorente, M.A. Vincenzo, Solid State Ionics 130 (2000) 91.
[16] B.W. Flynn, A.E. Owen, J.M. Robertson, Proc. 10th Int. Conf. on Amorphous and Liquid, Semiconductors, 1977, p. 678.
[17] H. Mori, H. Matsuno, H. Sakata, J. Non-Cryst. Solids 276 (2000) 78.
[18] D. Souri, J. Non-Cryst. Solids 356 (2010) 2181.
[19] T. Sankarappa, M.P. Kumar, G.B. Devidas, N. Nagaraja, R. Ramakrishnareddy, J. Mol. Struct. 889 (2008) 308.
[20] V.K. Dhawan, A. Mansingh, M. Sayer, J. Non-Cryst. Solids 51 (1982) 87.
[21] N. Chopra, A. Mansingh, G.K. Chadha, J. Non-Cryst. Solids 126 (1990) 194.
[22] H. Hirashima, M. Ide, T. Yoshida, J. Non-Cryst. Solids 86 (1986) 327.
[23] G.A. Chase, C.J. Phillips, J. Am. Ceram. Soc. 47 (1964) 467.
[24] H. Sakata, M. Amano, T. Yagi, J. Non-Cryst. Solids 194 (1996) 198.
[25] M. Nlyaz Ahamad, R. Vaish, K.B.R. Varma, J. Therm. Anal. Calorim. 105 (2011) 239.
[26] G.R. Jones, I.M. Young, J.W. Burgess, C. O'Hara, R.W. Whatmore, J. Phys. D Appl. Phys. 13 (1980) 2143.
[27] D. Xiao, S. Wang, E. Wang, Y. Hou, Y. Li, C. Hu, L. Xu, J. Solid State Chem. 176 (2003) 159.
[28] S. Sakida, S. Hayakawa, T. Yoko, J. Phys. Condens. Matter 12 (2000) 2579.
[29] J. Darriet, J. Galy, Cryst. Struct. Commun. 2 (1973) 237.
[30] V. Dimitrov, J. Solid State Chem. 66 (1987) 256.
[31] S. Rada, M. Rada, E. Culea, Spectrochim. Acta A 75 (2010) 846.
[32] Y.Z. Yue, J.deC. Christiansen, S.L. Jensen, Chem. Phys. Lett. 357 (2002) 20.
[33] Q. Zheng, M. Potuzak, J.C. Mauro, M.M. Smedskjaer, R.E. Youngmann, Y.Z. Yue, J. Non-Cryst. Solids 358 (2012) 993.
[34] L. Lutterotti, R. Ceccato, R.D. Maschio, E. Pagani, Mater. Sci. Forum 278–281 (1998) 87.
[35] K. Levenberg, Q. Appl. Math. 2 (1944) 164.
[36] D.W. Marquardt, J. Soc. Ind. Appl. Math. 11 (1963) 431.
[37] L.F. Maia, A.C.M. Rodrigues, Solid State Ionics 168 (2004) 87.
[38] N.F. Mott, Adv. Phys. 16 (1967) 49.
[39] I.G. Austin, N.F. Mott, Adv. Phys. 18 (1969) 41.
[40] M.A. Sidkey, R. El Mallawany, R.I. Nakhla, A. Abd El-Moneim, J. Non-Cryst. Solids 215 (1997) 75.
[41] N.M. Beekmans, L. Heyne, Electrochim. Acta 2 (1976) 303.
[42] J.E. Bauerle, J. Phys. Chem. Solids 30 (1969) 2657.
[43] G. Bruce, A.R. West, J. Electrochem. Soc. 130 (1983) 918.
[44] K. Shida, R. Sahara, M.N. Tripathi, H. Mizuseki, Y. Kawazoe, Mater. Trans. 50 (2009) 2848.
[45] R. Zallen, The Physics of Amorphous Solids, Wiley-VCH, 1998.
[46] M.N. Rahaman, Ceramic Processing and Sintering, CRC Press, 2003.
[47] I.J. Youngs, J. Phys. D Appl. Phys. 35 (2002) 3127.
[48] M. Sahimi, B.D. Hughes, L.E. Scriven, H.T. Davis, J. Phys. C Solid State Phys. 16 (1983) L521.
[49] A. Huanosta, A.R. West, J. Appl. Phys. 61 (1987) 5386.